

RESEARCH

Open Access



Development of highly efficient niosomal systems for co-delivery of drugs and genes to treat breast cancer in vitro and in vivo

Najmeh Alsadat Abtahi¹, Seyed Morteza Naghib^{1*}, Fatemeh Haghirsadat^{2*} and Mohammadmahdi Akbari Edgahi^{3,1}

*Correspondence:
Naghib@iust.ac.ir;
fhaghirsadat@gmail.com

¹ Nanotechnology Department, School of Advanced Technologies, Iran University of Science and Technology, Tehran, Iran

² Medical Nanotechnology & Tissue Engineering Research Center, Yazd Reproductive Sciences Institute, Shahid Sadoughi University of Medical Sciences, Yazd, Iran

³ Biomaterials and Tissue Engineering Department, Breast Cancer Research Center, Motamed Cancer Institute, ACECR, Tehran, Iran

Abstract

In this paper, we step forward in optimizing the efficiency of niosomal systems for carrying curcumin and miR-34a as single-/co-delivery to treat breast cancer. Curcumin, via regulation of p53 protein, affects the molecular signaling pathways and leads to cell death. Likewise, miRNAs, via alternation of the expression of genes, can suppress the development of tumor activities. To conquer and optimize the delivery limitation of curcumin and miRNA, niosomal systems with certain compositions (seven formulations) of Tween-80:Tween-60:cholesterol:DOTAP:PEG are introduced, which enhances the carrier size, surface charge, entrapment efficiency, transfection, and drug release. The results showed that Tween-60 has a significant influence on the entrapment efficiency of the composition. By including the PEG and DOTAP, high enhancements in the overall characteristics of the delivery system were observed. To assess the biological activity of samples, with/without the niosomal delivery system, cytotoxicity, apoptosis, in-vitro, and in-vivo cellular uptake were studied. The recorded data revealed better results from niosomal carriers than their free forms. The best result in single delivery was achieved by miRNA in F6, which had the highest apoptosis, uptake, and smallest tumor volumes under a controlled release. In conclusion, we successfully designed a nanoscale niosomal system to carry drugs and genes to the tumor site to treat cancer cells and provided remarkable data for the scientific society.

Keywords: Drug delivery, Curcumin, miRNA, Nanoniosome, Codelivery, Breast cancer

Introduction

Today, breast cancer is of the most common cancers among women, and even 25% of all female malignancies are diagnosed in developed countries (Mazidi et al. 2022; Yaghoubi et al. 2021; Abtahi et al. 2021, 2022; Naghib et al. 2020). It has been announced breast cancer is the second cancer-related death in women (Sadeghi et al. 2022a, 2022b; Rahimzadeh et al. 2021). Recent strategies for breast cancer therapy include surgery, chemotherapy, and radiotherapy (Urruticoechea et al. 2010; Rygiel 2017). Therefore, this implies better comprehension of genetic and biochemical factors in the uncontrolled proliferation of cells in the breast to treat such cancers



with innovative therapies (Xiang et al. 2019). There is growing interest in the development of nano-sized drug delivery systems to maximize the beneficial parameters (e.g., encapsulation and adsorption of therapeutic compounds) while minimizing the side effects (Gooneh-Farahani et al. 2019). Recent therapeutic compounds to combat breast cancer have led to the utilization of curcumin and miR-34a (Abtahi et al. 2022, 2021).

Curcumin (Cur) is a traditional spice, as well as medicine in many Asian countries, and it has an extended range of medical applications as anti-inflammatory, antioxidant, anti-amyloid, and antitumor (Abtahi et al. 2021; Yaghoubi et al. 2022, 2021). Cur is made from the extraction of rhizomes of turmeric (*Curcuma longa*), which is also known as yellow polyphenol or diferuloylmethane (Yaghoubi et al. 2022, 2021b). Moreover, some investigations have revealed that Cur has the potential to induce cell cycle arrest and/or apoptosis to block the activation of nuclear factor kappa B (NF- κ B) in various human cancers (Li et al. 2017).

Technically, microRNAs (miRNAs) are non-coding RNA molecules with ~17–23 nucleotides long, which occur naturally and they consist of a new category of ‘master regulators of gene expression (Portnoy et al. 2011). Almost in all solid and hematological malignancies, miRNAs are dysregulated, and specific miRNAs expression signatures that permit the characterization of various tumors and stages are destroyed (Moga et al. 2019). Therefore, miRNAs can be utilized as a diagnosis or prognosis in cancer therapy. Upregulated miRNAs are used in cancer cells and contribute to carcinogenesis by restricting tumor suppressor genes named oncogenic miRNAs. In contrast, down-regulated miRNAs, which prevent cancer growth by restricting the expression of proto-oncogenes, are named tumor suppressor miRNA (Sassen et al. 2008). The miRNA-34 family, which is defected in almost half of the human cancers, has a crucial role in combating tumor development (Cha et al. 2012). By transferring miR-34 mimics to cancer cells, prevention and inhibition of cancer cells growth were observed, which confirms the use of miRNA mimics in cancer treatments (Reid et al. 2016). Among this family, p53 is of the strongest inducers. The p53 protein is a regulator that multiplies the cellular pathways in response to genotoxic stress as well as upregulation of miRNA-34a in human and mouse cells as a consequence of DNA damage (Krstic et al. 2018). Likewise, miRNA-34a (miR-34a) was shown to be hypermethylated in breast, colon, and lung cancers (Li et al. 2014). In addition, ectopic miR-34a induces a G1 cell cycle arrest, senescence, and apoptosis, thereby possessing the tumor-suppressive role of miR-34a (Adams et al. 2016).

For this purpose, nanotechnology has dramatically changed the diagnoses or treatments of cancer (Mazidi et al. 2022). Nanotechnology with a nano-DDS can diagnose and treat breast cancer by delivering therapeutic or diagnostic agents to the target sites (Marta et al. 2016). Niosome carriers are obtained from self-accumulation of non-ionic surfactants in a medium which ultimately forms an enclosed bilayer lipid structure (Naderinezhad et al. 2017; Hemati et al. 2019). In addition, these carriers primarily contain non-ionic surfactants and additives (Majdizadeh et al. 2018). They can entrap water-soluble molecules within an aqueous environment by their spherical lipid bilayers. Moreover, regarding the preparation method, these carriers may be unilamellar or multilamellar depending. The potential of the niosomes has been widely studied to be

exploited as carriers for the delivery of drugs, antigens, hormones, and other bioactive agents for a specific period or organ of the body (Abtahi et al. 2022, 2021).

In this study, we developed new compositing ratios of Tween-60:Tween-80:cholesterol with/without the addition of DOTAP and PEG to optimize the general characteristics of niosomal carries by maximizing the entrapment efficiency of curcumin and miRNA, facilitating the adsorption of the therapeutic compounds as single-/co-delivery with controlled-release, and minimizing the side effects while maintaining the current state for prolonged storage. To evaluate the properties of the synthesized carriers, their size, zeta, PDI, EE%, R%, and stability were measured. The cytotoxicity, apoptosis, in-vitro, and in-vivo tests were conducted, and the results were listed and discussed in the following sections.

Materials and methods

Materials

Tween-60, Tween-80 (DaeJung Chemicals & Metals, Seoul, South Korea), curcumin, DOTAP (1,2-dioleoyl-3-trimethylammonium-propane), cholesterol (Sigma-Aldrich, St. Louis, MO), DPPC (1, 2-dipalmitoyl-sn-glycerol-3-phosphocholine phospholipid), DSPE-PEG2000 (distearoyl phosphoethanolamine-polyethylene glycol, Lipoid GmbH, Ludwigshafen, Germany) were acquired for this study. The rest of the reagents used were of analytical grade and have not been further purified unless mentioned. The sequences of the miR-34a targeted were sense Forward primer AGTCTAGAGCCACCGTCCA, Reverse primer TCTGACGCACACCTATTGCAAGC.

Preparation of niosomal nanoformulations

Cur-loaded niosomes were synthesized by the thin-film technique. In this case, various molar concentrations of Tween-60, Tween-80, and cholesterol were suspended in chloroform. First, Cur was dispersed entirely in methanol with a 1:2 (mg/mL) ratio. Then, the solution was transferred to the mixture of surfactant and lipid; then a rotary flash evaporator was employed (Heidolph, Germany) to evaporate the solution at 60 °C for 1 h. Afterward, 3 mL of phosphate-buffered saline (PBS) with pH 7.4 was used to hydrate the lipid-formed film. Ultimately, to diminish the scale of the particles, a microtip probe sonicator was employed (E-Chrom Tech Co., Taiwan) to sonicate the solution for 30 min. To split unloaded Cur, first, 12 kDa MWCO dialysis bags were applied to dialyze the solution. The primary Cur of 500 µg was calculated as the optimal amount, while the ratios of cholesterol, Tween-60, and Tween-80 were different in nanoparticles. Next, the volume of DOTAP was optimized. Cationic niosome was made in a similar procedure to deliver miRNA and Cur at different ratios. To verify the formed ratios between niosomal Cur and miR-34a, a gel retardation assay was performed. In addition, in each step, controlled release parameters, encapsulation efficiency, and particle size were analyzed. Further investigations showed that formulation number 5 (F5) was the optimal one.

Characterization of particles

To analyze the characterization of particles, poly-dispersity index (PDI), and zeta potential, a dynamic light scattering was employed (DLS, Brookhaven Instruments, Holtville, New York, USA). The results and mean values were reported for a triplicate

measurement. In addition, AFM was conducted (AFM5100N, HITACHI) to analyze the morphology of the Cur-loaded niosomes.

Encapsulation efficiency of the particles

For gauging the amount of encapsulated Cur, after removing unencapsulated Cur as mentioned above, they were soaked in PBS at 4 °C and lysed with isopropanol to the niosomes. To quantify the drug release rate (R%), a UV–Vis spectrophotometer at 429 nm wavelength was employed (T80+, PG Instruments, UK). The following equation was utilized to measure the encapsulation efficiency:

$$\text{Encapsulation efficiency (EE, \%)} = \frac{\text{The quantity of Cur capsulized inside niosomes}}{\text{The total quantity of Cur added}} \times 100$$

In-vitro release of pH-/thermo-sensitive curcumin

12 kDa cutoff dialysis tube was performed in the PBS at various temperatures (25, 37, 42 °C), and 5.5 and pH 7.4 for 72 h while magnetically stirring at 70 r.p.m. for measuring the released Cur from niosomes. At the different intervals, a small quantity of each experiment was collected and analyzed by UV–Vis spectrophotometer to calculate the release rate. In addition, to maintain the condition, after the removal, the same amount of fresh PBS was immediately added.

Functional group characterization

To assess the interaction between therapeutic compounds and carrier molecules, Fourier Transform Infrared spectroscopy (FTIR) was performed (8300, Shimadzu Corporation, Tokyo, Japan). For this purpose, each sample was converted to dry powder by lyophilizing and then blended with potassium bromide (KBr). Ultimately, samples were hydraulically pressed and created the pellets.

Physical stability analyses

After calculating the particle diameter, residual quantity, zeta potential, and PDI of the therapeutic compounds, the Cur-loaded niosome within 15~60 days were analyzed to measure their physical stability inside the vesicle.

Synthesis of miRNA-loaded niosomal complexes

The complex formation between miR-34a and cationic niosomes was obtained by a gel retardation assay. The miR-34a and cationic niosomes can be combined in a dosage-dependent condition. Thereby, the optimal condition was a 133:1 ratio of cationic niosomes:miR-34a. To assure the loading of miRNA onto cationic niosomes, zeta potential analysis was obtained before and after the loading. For calculating the long-term storage impacts, all formulations were maintained at 4 °C for 4 months, and then, the leakage of miR-34a was assessed.

Cytotoxicity study

To analyze the biocompatibility, an MTT test for each formulation was performed to measure the level of cytotoxicity. For this purpose, 96-well plates were used, and both

cancer and healthy cells were seeded at 1×10^4 cells/well. After 1 day, 200 μL of different concentrations of niosomal curcumin (NCur), free curcumin (fCur), niosomal miR-34a (NmiR), and free miR-34a (fmiR) were added to each sample. Afterward, all samples were incubated at 37 °C for 1, 2, and 3 days. Then, 20 μL of MTT (5 mg/mL in PBS) were inserted in all samples and followed by another incubation for 3 h. Ultimately, the medium was extracted with care, and to dissolve formazan crystals, as well as insertion of 180 μL of DMSO into each sample. To record the adsorb rate, an EPOCH microplate reader at 570 nm was utilized (synergy HTX, BioTek, USA). All the results from the MTT assay were obtained by GraphPad Prism 6 software and stated as the Inhibitory Concentration (IC₅₀) value, which shows the level of inhibition of cell growth by 50% according to the drug concentration compared to the controls.

In-vitro cellular uptake

First, cells at 2×10^5 cells/well concentration were seeded and incubated in a 6-well plate for 1 day. Then, cells were treated with various solutions, including NCur, NmiR, NCur + NmiR, NCur/NmiR, fmiR, fCur, and unloaded niosomes, followed by incubation for 3 h. Next, samples were washed three times with cold PBS and soaked in paraformaldehyde solution (4%, Sigma, USA), respectively. 0.125 $\mu\text{g}/\text{mL}$ of 4',6-diamidino-2-phenylindole (DAPI) (Thermo Fisher Scientific, USA) was utilized to stain the cells' nucleus. Technically, miR-34a and Cur emit red and green-colored fluorescence signals, respectively. Herein, for taking the images, a fluorescence microscope was used (BX61; Olympus: Japan) (Alemi et al. 2018; Lv et al. 2014; Lin et al. 2012).

Apoptosis assay

To measure the apoptosis of cells, first, 1×10^5 cancer cells/well concentrations were seeded into 6-well plates. Then, cells were subjected to NCur, fCur, NmiR, and fmiR (Fc4, Fc5, Fc6) at their IC₅₀ value and incubated for 1 day. Next, to detach the cells 0.25% trypsin/EDTA (Sigma-Aldrich, USA), centrifugation at 1500 r.p.m. for 3 min, suspension of the pellet in the ice-cold PBS at pH 7.4 were performed, respectively. Ultimately, according to the annexin V-FITC/PI (Sigma-Aldrich, USA) double staining procedure, 3 μL of annexin V-FITC and propidium iodide stock solutions were included in the suspension to detect apoptotic and necrotic cells, respectively. After 30 min of ice incubation, samples were assessed by flow cytometry (BD FACSCalibur instrument).

In-vivo experiments

The animal experiment was conducted according to NIH and IACUC guidelines. Thirty-five 6–8-week-old female BALB/c mice (Pasteur Institute, Iran) with 20–25 g weight were acquired and held in a sterilized condition. To prepare the mice, 5×10^6 4T1 cells were subcutaneously inoculated into the right flank of each mouse. Then, as the tumor grew to approximately 100 mm^3 , they were categorized into 7 groups of 5 mice. The injection of fCur, fmiR, NCur (Fc4, Fc5, Fc6), and NmiR, as well as normal saline for the control group, was performed in the tail vein of the animals. The dosage of free medicines and niosomal medicines was 2.5 mg/kg and 10 $\mu\text{g}/\text{mouse}$, respectively. The injection was repeated every 3 days until 12 days. The body and tumor size of the mice were

calculated every 3-day intervals, and they were sacrificed on the last day. According to the following equation, the tumor size was determined:

$$V[\text{mm}^3] = \frac{1}{2} \times LW^2$$

where L and W represent the long and short lengths of the tumor, respectively. In addition, the following formula was employed to measure the tumor inhibition rate:

$$\text{Tumor Inhibition Rate (TIR, \%)} = \left[\frac{(W_c - W_t)}{W_c} \right] \times 100$$

where W_c and W_t represent the average weight of the tumor in the control and treated groups, respectively.

Statistical analysis

To prepare statistical data and comparisons, GraphPad Prism 6, an ANOVA test, and a student t test were employed and the results were exported as mean \pm SD. A $p < 0.05$ was statistically significant.

Results

The influence of surfactants and reagents

For optimizing the Cur formulation, several parameters including R% (24 h and 37 °C), EE%, and vesicle size, were assessed. According to the results listed in Tables 1 and 2, the first formula (F1) had the lowest EE% and R% and largest particle size, but in F2, by swapping the Tween-80 and Tween-60 compositing ratio, a modest improvement was observed. While a certain amount of Tween-60 adds to the Tween-80 and cholesterol as the F3, significant promotion in EE%, particle size, and PDI was obtained, but no notable change was observed in zeta potential. Therefore, regarding the optimal parameters for both drug and gene delivery systems, the F3 has been selected for our future study.

The influence of DOTAP and DSPE-mPEG (2000)

Changing the quantity of Tween-80 and Tween-60 from the F3 to F6 by the addition of DOTAP and PEG to the composition, remarkably enhanced the total performance of the system. To attain smaller niosomes, improve stability, higher entrapment efficiency, and less aggregation, 5% PEG was added as F4. Based on the results, a smaller PDI, smaller diameter, higher drug entrapment, and a more negative charge were observed in the F4 than in the aforementioned formulas. Moreover, by including DOTAP in the formulations, the entrapment efficiency and positive charge particles were enhanced, while the PDI and vesicle size decreased. Overall, among all NCur formulations, F6.1 containing Tween-80:Tween-60:cholesterol:DOTAP:PEG with a 65:12.5:7.5:10:5 molar ratio demonstrated favorable characteristics, including improved transfection efficiency, small diameter, high entrapment efficiency, and sustained drug release. Thus, further investigation has been performed, and the characterization of both F6 has been analyzed by AFM imaging. The result of the AFM analysis was displayed in Fig. 1a–f. Figures demonstrated pegylated, sphere-shaped, globular, and smooth nanoparticles without considerable aggregation. However, the F7 shown in Table 3 with a 60.5:12.5:7:15:5 molar

Table 1 Effects of Tween-80:Tween-60:cholesterol:DOTAP:PEG ratios on the EE%, PDI, R%, diameter size (nm), and Zeta potential (mV) of the Cur-loaded system

Code	Tween-80	Tween-60	Cholesterol	DOTAP%	PEG%	EE%	PDI	Zeta (mv)	Diameter (nm)	R% (24 h, 37 °C)
F1	90	0	10	-	-	30.43	0.24 ± 0.003	- 25 ± 0.02	120 ± 0.03	8 ± 0.23
F2	0	90	10	-	-	50.14	0.27 ± 0.24	- 24 ± 0.15	117 ± 0.98	15 ± 0.23
F3	75	15	10	-	-	78.34	0.21 ± 0.16	- 24 ± 0.34	110 ± 0.45	19 ± 0.67
F4	70	15	10	-	5	85.34	0.19 ± 0.48	- 25 ± 0.67	101 ± 0.56	21 ± 0.78
F5	70	15	10	5	-	90.66	0.17 ± 0.19	+ 5 ± 0.45	93 ± 0.34	28 ± 0.56
F6.1	65	12.5	7.5	10	5	99.85	0.15 ± 0.067	+ 16 ± 0.67	86 ± 0.67	33 ± 0.48

Table 2 Effects of Tween-80:Tween-60:cholesterol:DOTAP:PEG ratios on the PDI, diameter size (nm), and Zeta potential (mV) of the miRNA-loaded system

Code	Tween-80	Tween-60	cholesterol	DOTAP%	PEG%	PDI	Zeta (mv)	Diameter (nm)
F1	90	0	10	–	–	0.21 ± 0.12	– 22 ± 0.13	116 ± 0.44
F2	0	90	10	–	–	0.23 ± 0.42	– 21 ± 0.44	113 ± 0.98
F3	75	15	10	–	–	0.19 ± 0.005	– 23 ± 0.65	100 ± 0.023
F4	70	15	10	–	5	0.18 ± 0.36	– 27 ± 0.098	95 ± 0.033
F5	70	15	10	5	–	0.15 ± 0.65	+ 15 ± 0.53	81 ± 0.004
F6.2	62.5	12.5	7	15	5	0.13 ± 0.045	+ 23 ± 0.11	72 ± 0.42

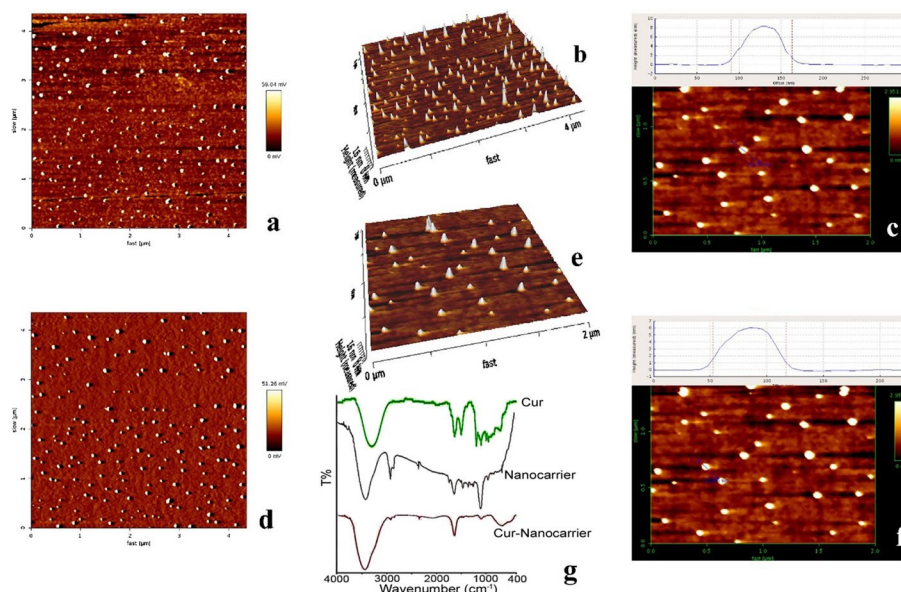


Fig. 1 AFM images of **a** and **d** 2D, **b** and **e** 3D, **c** and **f** line analysis of NCur NPs. **c, f** Influence of individual variables on the carrier diameter. **g** FTIR spectra of Cur, nanocarrier and nanocarrier loaded Cur

Table 3 Effects of Tween-80:Tween-60:cholesterol:DOTAP:PEG ratios on the PDI, diameter size (nm), and Zeta potential (mV) of the Cur- and miRNA-loaded system

Code	Tween-80	Tween-60	cholesterol	DOTAP%	PEG%	PDI	Zeta (mv)	Diameter (nm)
F7	60.5	12.5	7	15	5	0.15 ± 0.067	+ 10 ± 0.001	85 ± 0.015
	miR-34a							

ratio possessed the optimal characteristic regarding the small diameter and more positive charge. Fourier-transform infrared spectroscopy (FTIR) was conducted to evaluate the presence of Cur in nanoniosomes. In Fig. 1g, FTIR spectra of Cur, nanocarrier and Cur-nanocarrier were shown. In the Cur spectra, the bands at 800–600/cm were attributed to the C–H out plane bending vibrations, 1152/cm to C=O stretch, 1,506/cm to aromatic ring C=C stretching, and 3507/cm to O–H and C–H stretching. In the nanocarrier, various peaks around 3500–1,115/cm were detected which was attributed to the O–H stretching in phenols and N–H stretching in 2°-amines in Tween-60 and

cholesterol at 3,435/cm, C–O stretch in Tween-60 at 1148/cm, and C=O robust absorption at 1642.15/cm because of C–O stretching vibration in Tween-60. As a comparison to Cur-nanocarrier, the broader bands at 3500 and 500–900/cm, and the sharper band at 1600/cm, validated the presence of Cur in the delivery system. Therefore, FTIR analysis confirmed the presence of the drug in the nanocarrier.

In-vitro drug release study

The release profile of Cur was investigated in PBS at 25, 37, and 42 °C, and 5.5 and 7.4 pH (Fig. 2). Whereas the pH of the extracellular and intracellular of the cancer cells are lower and higher compared to the healthy cells, respectively. Therefore, both neutral and acidic pH conditions were used to investigate the release profile of the drug. The results showed that temperature could highly affect the release of Cur in F4, F5, and F6 at both testing pHs. First, a rapid release phase of the drug was observed and then reduced in

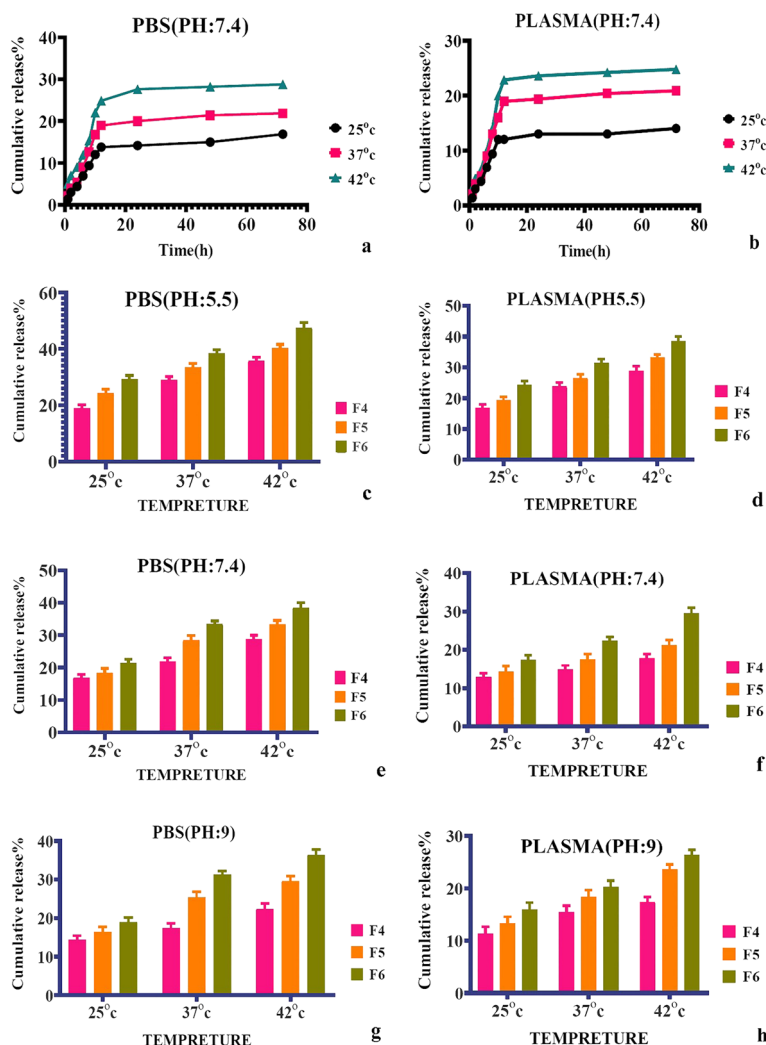


Fig. 2 Influence of temperature on optimal NCur release in **a** PBS and **b** Plasma at pH:7.4. The influence of multiple formulations Cur in PBS at pH **c** 5.5, **e** 7.4, and **g** 9. The influence of multiple formulations of NCur in plasma at pH **d** 5.5, **f** 7.4, and **h** 9

the next phase. The maximum release was observed at 42 °C and acidic pH. In addition, in all conditions, F6 had a higher release rate than F4 and F5. After adding DOTAP, the unsaturated alkyl chain increase the flexibility of binding, so it is more mobile and flexible; as a result, the drug release is enhanced (Cha et al. 2012). Technically, in temperatures higher than 42 °C, the bilayer membrane permeability of niosomes changes which results in a higher release rate. Moreover, in a more acidic environment, a proton gradient is formed across the membrane, which increases the release rate (Reid et al. 2016).

Physical stability examination

Cur has low solubility, which restricts its applications. To overcome and promote the drug's bioavailability and stability, miR-34a and Cur were incorporated into cationic niosomes. In general, it is crucial for a drug to maintain its stability after a long storage period. Thus, to keep their high stability, the effect of zeta potential and particle size were investigated. In addition, barriers between vesicular particles were created to prevent accumulation (Krstic et al. 2018). For measuring the changes in the PDI, size of the vesicles, EE%, and zeta potential, of the NmiR (Fm) and NCur carrier (Fc4, Fc5, and Fc6) were preserved at 4 °C for 15, 30, 45, and 60 days. The results displayed no considerable alteration in F6c and F7 compared with newly synthesized systems (p value < 0.05), which confirms the total stability of NCur after 2 months. Similarly, these results were repeated for miRNA niosomes. Thus, the addition of DOTAP to the composition can promote physical stability (Fig. 3).

Synthesis of miRNA-loaded niosomal complexes

A gel retardation assay was employed to measure the complex formation between miRNA and cationic niosomes. In Fig. 3e, the dosage-dependent approach of binding cationic niosomes to miRNA was displayed. According to the observations from the electrophoresis test, miRNA-loaded niosome formulation is stable, and can form a complex at the ratio of 1:136. As mentioned in Table 2, zeta potential analysis was conducted before and after the loading of miRNA to confirm the binding of cationic niosomes to miRNAs. Herein, both complex formation and electrostatic bonding are able to expand the size between the two parties. In addition, the connection of the long chains of miRNA to the niosome surface builds a spatial barrier that leads to the promotion of hydrodynamic diameter. Yet, the diameter in the final formulations was less than 100 nm. Ultimately, after 4 months of storage at 4 °C, the lowest leakage was observed.

Cytotoxicity study

The cytotoxicity of Cur was analyzed in both fCur and NCur (Fc4, Fc5, Fc6) states via measuring the cell viability of cancer cells. In addition, the IC₅₀ values were calculated after 48 and 72 h (Table 4, Fig. 4). Moreover, the cytotoxicity of NCur was higher than fCur. Whereas after 72 h of incubation, the difference became significant.

The unloaded niosomes demonstrated no cytotoxicity on the cell viability. While fCur and NCur restricted the development of cancer cells. In addition, while cancer cells were targeted by niosomal nanoformulation, the inhibitory impact was significantly increased. Therefore, it was concluded that miR-34a and Cur have synergetic roles in the

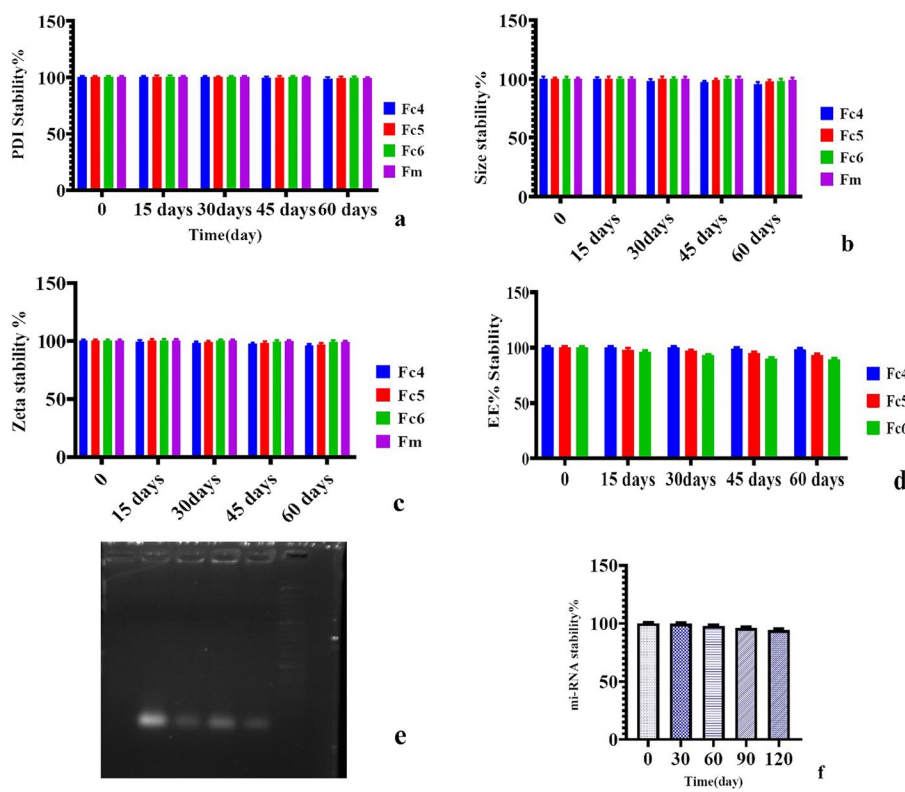


Fig. 3 Obtained stability of formulation of Cur (Fc4, Fc5, Fc6) according to **a** PDI test, **b** size, **c** zeta, and **d** EE%. **e** Synthesis of cationic miRNA-loaded niosomal complexes and **f** their time-dependent stability

Table 4 IC50 values of fCur and NCur states on cancer cells after 48 and 72 h

Time	fCur	Fc4	Fc5	Fc6
48 h	0.1704 ± 0.001	0.1463 ± 0.008	0.1188 ± 0.005	0.1012 ± 0.004
72 h	0.091 ± 0.004	0.091 ± 0.003	0.084 ± 0.009	0.061 ± 0.002

elimination of cancer cells. The cooperation of miR-34a and Cur in the niosomal nano-formulation states can promote the total therapeutic effect of the drug.

Cellular uptake assay

To perform the cellular uptake assay, a fluorescence microscope was employed and cancer cells as a cancerous model were utilized (Figs. 4 and 5). In this case, cancerous samples were exposed to various formulations (Fc4, Fc5, Fc6, Fm, fCur, and miR-34a). By exposing the cells to fCur or NCur, green-colored light was emitted. In contrast, the ones that were exposed to the fmiR or NmiR emitted red-colored light (Figs. 4 and 5). However, the cells treated with nanoformulations of niosomes demonstrated higher fluorescence intensity than the gene, drug, and free states. It was observed that when miR-34a was accumulating in the cytoplasm, the nucleus region and cytoplasm had already accumulated with Cur. In addition, it was observed higher fluorescence intensity by Fc6 than other Cur formulas and Fc5 than Fc4. In this test, cationic

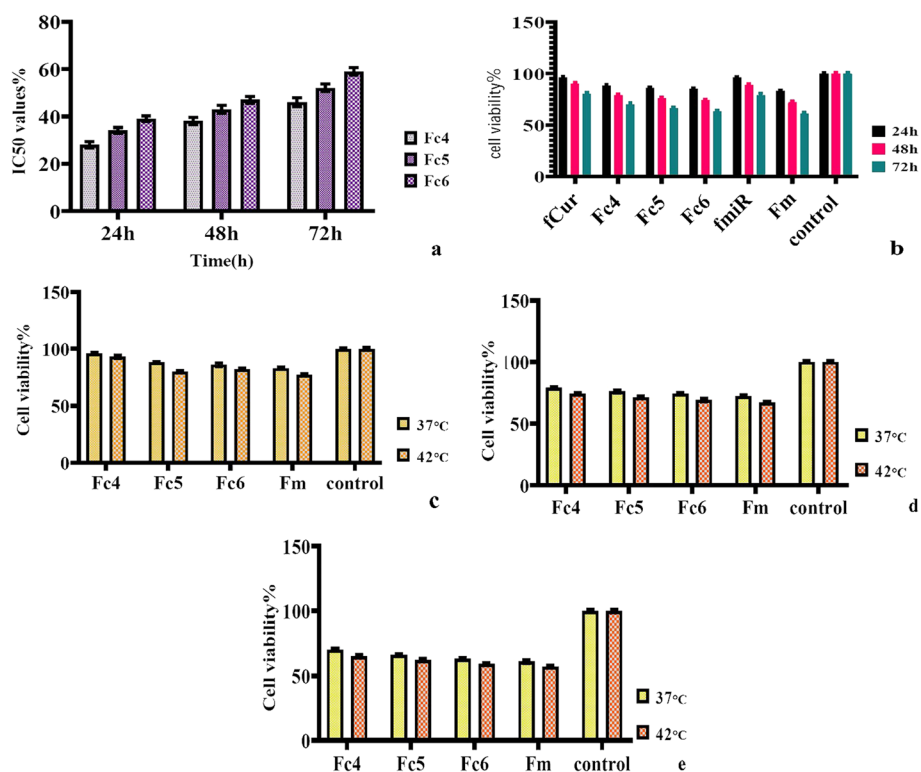


Fig. 4 **a** IC50 analysis of various formulations of fCur and NCur in cancer cells. **b** Measured live cancerous cells were treated by the fCur, NCur, and NmiR. **c** Measured live cancerous cells treated by niosomal NPs at 37 and 42°C for 24 h. **d** Cell viability of the niosomal NPs in cancerous cells at 37 and 42°C for 48. **e** Cell viability of the niosomal NPs in cancerous at 37 and 42°C for 72 h

niosomes were successfully uptook by the cancerous cells. Technically, in the penetration of NCur in the cells, endocytosis plays an essential role by transferring the miRNA and Cur into the cells, while fCur uses a diffusion mechanism to pass through the cells’ membranes. This insertion was facilitated due to the utilization of niosomes as a hydrophilic drug carrier.

Gene expression

The expression level of p53 and Nf-κB was evaluated to examine the efficiency of miR-34a’s targeting and confirm the downstream impact of miRNA gene silencing. Herein, qRT-PCR methods were performed to detect the Nf-κB and p53 expression. For this purpose, after exposing cells to fCur, NCur, fmiR, and miR, the expression of the NF-κB genes and P53 in the cells were examined. Results showed that both fCur and fmiR slightly reduced the gene expression of NF-κB and enhanced the expression of p53 compared to the control group (Fig. 6a, b). Moreover, the changes in the gene expressions were significantly greater in NCur and NmiR than fCur and fmiR, respectively. Ultimately, the highest results in gene expressions were observed when miRNA and Cur were utilized in either free or niosomal states. While on the cancerous cell, Fc6 demonstrated better gene expression than Fc5 and Fc4.

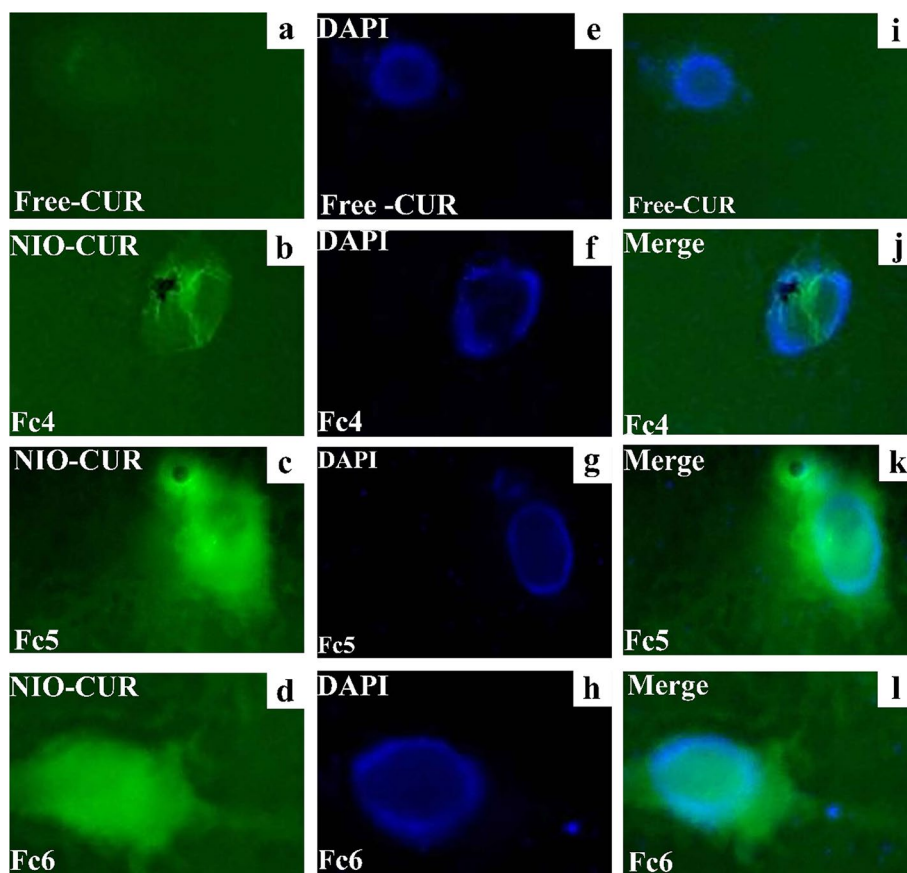


Fig. 5 Cellular uptake images of Free-CUR, Fc4, Fc5 and Fc6

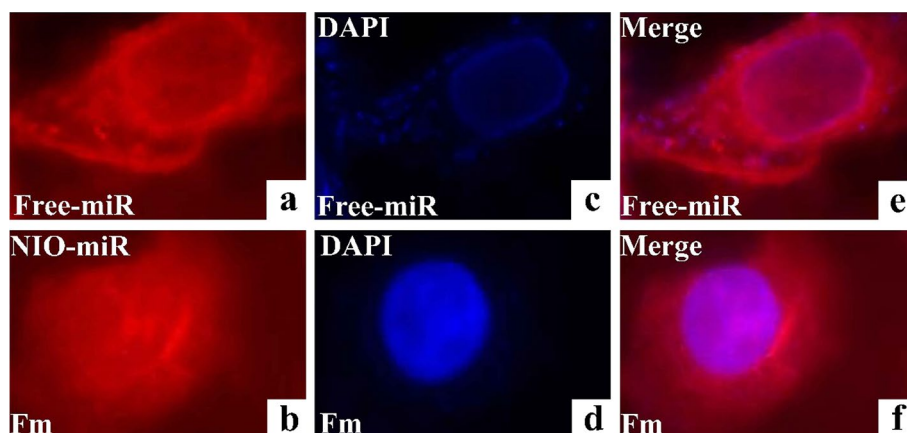


Fig. 6 Cellular uptake images of Free-miR and Fm

Apoptosis analysis

Annexin V-FITC/PI double staining assay was performed to evaluate the apoptosis rate of each delivery system after 1 day. After apoptosis of the cell, the membrane changes, and phospholipid phosphatidylserine (PS) shifts from inward to outward, which subjects itself to the exterior environment. Then, the PS interacts with annexin

V which is a 35–36 kDa calcium-dependent phospholipid-binding protein. To promote the interaction level and affinity of annexin V to PS, it was conjugated to a fluorescent molecule, such as fluorescein isothiocyanate (FITC), which made annexin V-FITC. Similarly, propidium iodide (PI) is utilized as a DNA stainer that cannot penetrate into the alive or recently dead cells. After 2 days, the results were recorded (Fig. 6c). The results demonstrated a higher apoptosis rate using niosomal carriers compared to the free forms. In addition, miR-34a in both forms displayed a slightly higher death rate than in Cur forms. Among the formulations, Fc6 obtained the highest result.

In-vivo assessment of tumor inhibition rate

The anticancer activity of samples was evaluated by inoculation of 4T1 cells to the mouse models and waiting for the tumor to reach 100 mm³. Afterward, each group was subjected to medicine, and results were recorded every 3-day intervals. A digital vernier caliper was employed to measure the tumor sizes. The results revealed that both the drug and gene had a significant influence on tumor size. Smaller tumors were obtained using a niosomal delivery system (Figs. 7d and 8). By comparing the tumor inhibition capability of both drug and gene, in the same formulation, NmiR had the smallest tumor size of other forms, including fCur, NCur, and fmiR (Fig. 7b, c). Similarly, cytotoxicity was evaluated by weighing the mice at each interval, and the results are listed in Table 5 (Fig. 7a, b). According to the observations, the mice subjected to the therapeutic compounds had a slight reduction in their body weight after 21 days compared to the control group, which received normal saline. In addition, after 6 days, the lowest and highest weight reduction was observed in miRNA and Cur groups, respectively.

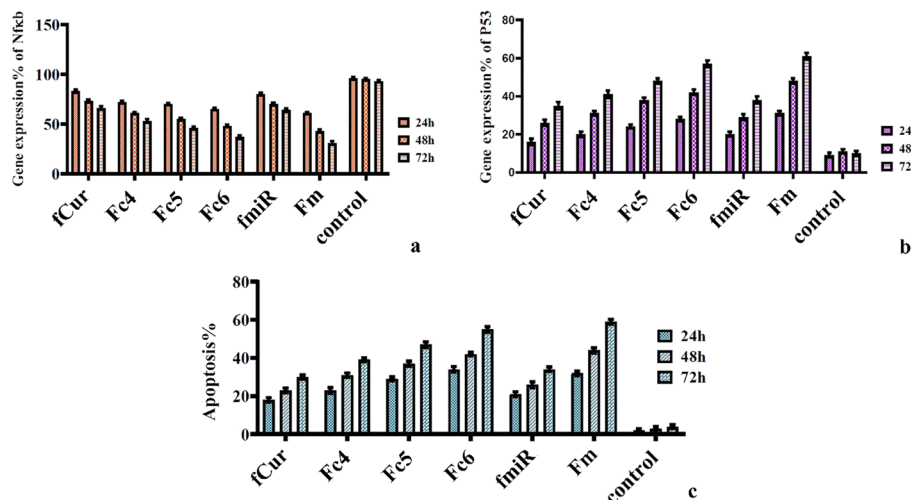


Fig. 7 Expression of **a** NF-κB and **b** p53 in real-time PCR analysis after being exposed to the formulations for 2 days. The measured dead cancerous cells in apoptosis assay after being treated exposed to the formulations for 1 day

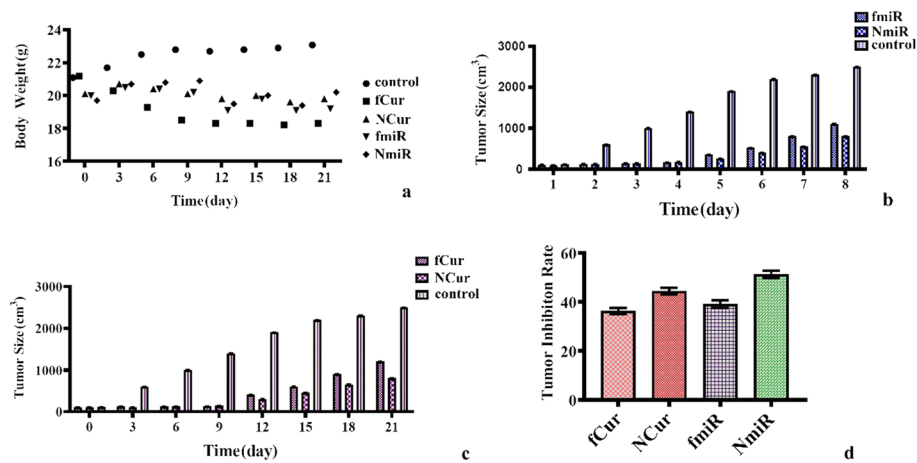


Fig. 8 **a** Effect of Cur and miRNA formulations on the bodyweight at every 3-day intervals, respectively. **b, c** Tumor size (cm³) of different mice groups after 21 days of receiving the medicine. All groups displayed a major decrease ($P < 0.05$) in the tumor volumes than the control group after 14 and 21 days. **d** Tumor inhibition rate

Table 5 Average body weight of each group of mice treated with different medicine at intervals

Duration (day)	fCur	NCur	fmiR	NmiR	Control
0	21 ± 0.05	21.1 ± 0.2	21 ± 0.4	21 ± 0.2	21.1 ± 0.4
3	20.1 ± 0.1	20.7 ± 0.6	20.2 ± 0.02	20.8 ± 0.5	21.7 ± 0.1
6	20.3 ± 0.2	20.1 ± 0.2	20.5 ± 0.1	20.2 ± 0.01	22.5 ± 0.4
9	19.7 ± 0.3	20.3 ± 0.1	19.7 ± 0.2	20.7 ± 0.6	22.6 ± 0.3
12	19.5 ± 0.3	19.3 ± 0.7	19 ± 0.7	20.2 ± 0.3	22.6 ± 0.1
15	19.5 ± 0.1	20 ± 0.3	20 ± 0.2	20.4 ± 0.02	23.4 ± 0.2
18	19.4 ± 0.5	19.8 ± 0.6	19.2 ± 0.5	20.1 ± 0.5	23.3 ± 0.4
21	19.1 ± 0.6	19.3 ± 0.1	19.2 ± 0.1	19.8 ± 0.1	23 ± 0.8

Discussion

By developing of drug delivery system and fabrication of advanced therapeutical compounds, in this paper, the efficacy of Cur as the drug and miR-34a as the gene models for treating breast cancer were evaluated. For drug carriers, nanoscale niosomes were chosen as their hydrophilic trait to facilitate the insertion into the cell membrane. The experiment showed that, for the fabrication of Cur, the ratio of Tween-60 has a major role in the entrapment of niosomes. The reason was that the mean diameter of Cur could be significantly influenced and reduced as a result of the higher ratio. F3 with 100 ± 0.023 nm diameter demonstrated notable entrapment, but when 5% PEG was added to the formulation without changing the Tween-60's ratio, despite the reduction of diameter to 95 ± 0.033 nm, the entrapped niosomes were increased. In addition, the addition of PEG has a major drawback on release rate due to the increase of negative charge as the pH of the intracellular matrix of cancer cells is high. Therefore, adding DOTAP to the formulation changed the charge, and consequently, the release rate in F5 and F6 was significantly enhanced.

As mentioned above, the pH of extracellular and intracellular cancer cells are different from normal cells, and when the sample was exposed to the adjacent environment of the

cancerous cells (more acidic), due to the formation of a proton gradient, the more positive charge formulation experienced higher release rate. However, when the temperature increased above 42 °C, it dysfunctionized the permeability of the niosome's bilayer and led to more release in all formulations. Subsequently, the presence of both positive charge and niosome promoted the cellular uptake via changing the penetration mechanism to endocytosis. Therefore, when cationic niosomes were loaded with either miR-34a or Cur, they displayed a more significant influence to restrict the development of cancer cells. The reason was that more adsorption of miR-34a and Cur could reduce the expression of NF- κ B and improve the p53 better than their free states. Besides, the best result was observed from F7 when both miR-34a and Cur were cooperating.

The same outcomes in biological activity were achieved according to the physical parameters. In the MTT test, the Fc6 of NCur had an IC50 value of 0.061 ± 0.002 after 72 h, which was the lowest and best compared to the fCur, Fc4, and Fc5 groups. Likewise, as it was displayed in Figs. 4 and 5, the higher in-vitro cellular uptake was obtained via the utilization of niosomal carrier, specially Fc6 in both drug and gene, than the free forms. However, the fluorescence intensity of red light emitted by miRNA treated cells was higher than Cur, which confirmed the higher affinity of genes to be adsorbed. This result was also confirmed in the apoptosis test (Fig. 6), where the expression of NF- κ B was higher than p53 protein in both forms.

Despite the differences in in-vitro assessments, the in-vivo test demonstrated almost close results. After 21 days of the subjection to normal saline and therapeutic compounds, fCur, fmiR, and NCur had relatively similar bodyweight around 19.2 g, but NmiR had a bodyweight of 19.8, which is the closest to the average mean weight of 21. Therefore, it can be concluded that the decrease in cell growth was the result of the constant inhibition by the samples.

Conclusions

In this experiment, we successfully fabricated a nanoscale niosomal system to facilitate the delivery of hydrophobic compounds, such as curcumin. Niosomal with a simple composition of Tween-80:Tween-60:cholesterol had several drawbacks, such as negative charge and particle size. Therefore, we added DOTAP to alter the charge to positive. In addition, by the addition of PEG, we obtained higher quality carriers based on all parameters mentioned above. Ultimately, Tween-80:Tween-60:cholesterol:DOTAP:PEG with the ratios of 65:12.5:7.5:10:5 for the drug and 62.5:12.5:7:15:5 for the gene demonstrated the highest physical properties. For biological assessments, we mainly focused on Fc4, Fc5, and Fc6. In spite of close outcomes, miRNA-containing Fc6 displayed the best results among the other testing groups. We hope that further modification of such carriers and medicines can completely secure the result and become a mainstream procedure for the treatment of breast cancer.

Abbreviations

Cur	Curcumin
NF- κ B	Nuclear factor kappa B
miRNAs	MicroRNAs
miR-34a	MiRNA-34a
DOTAP	1,2-Dioleoyl-3-trimethylammonium-propane
DSPE-PEG2000 or PEG	Distearoyl phosphoethanolamine-polyethylene glycol

PBS	Phosphate-buffered saline
PDI	Poly-dispersity index
R%	Release rate
EE%	Encapsulation efficiency
NCur	Niosomal curcumin
fCur	Free curcumin
NmiR	Niosomal miR-34a
fmiR	Free miR-34a

Author contributions

NAA, SMN and FH contributed to methodology, investigation and writing original draft. MAE helped in writing original draft, writing—review, editing and validation. All authors read and approved the final manuscript.

Funding

The authors state no funding involved.

Availability of data and materials

The data sets generated during and/or analyzed during the current study are available from the corresponding author on reasonable request.

Declarations

Ethics approval and consent to participate

This article only have animal subjects performed by the authors. Animal experiments were approved by the Animal Ethics Committee of Shahid Sadoughi University of Medical Sciences and were conducted in accordance with the policies of the Iran National Committee for Ethics in Biomedical Research (IR.SSU.MEDICINE.REC.1400.358).

Consent for publication

All authors agree to publication.

Competing interests

The authors state no conflict of interest.

Received: 17 May 2022 Accepted: 20 September 2022

Published online: 29 September 2022

References

- Abtahi NA, Naghib SM, Haghirsadat F, Reza JZ, Hakimian F, Yazdian F, Tofighi D (2021) Smart stimuli-responsive biofunctionalized niosomal nanocarriers for programmed release of bioactive compounds into cancer cells in vitro and in vivo. *Nanotechnol Rev* 10(1):1895–1911
- Abtahi NA, Naghib SM, Ghalekohneh SJ, Mohammadpour Z, Nazari H, Mosavi SM, Gheibihayat SM, Haghirsadat F, Reza JZ, Doulabi BZ (2022) Multifunctional stimuli-responsive niosomal nanoparticles for co-delivery and co-administration of gene and bioactive compound: In vitro and in vivo studies. *Chem Eng J* 429:132090
- Adams BD, Parsons C, Slack FJ (2016) The tumor-suppressive and potential therapeutic functions of miR-34a in epithelial carcinomas. *Expert Opin Ther Targets* 20(6):737–753
- Alemi A, Reza JZ, Haghirsadat F, Jalilani HZ, Karamallah MH, Hosseini SA, Karamallah SH (2018) Paclitaxel and curcumin coadministration in novel cationic PEGylated niosomal formulations exhibit enhanced synergistic antitumor efficacy. *J Nanobiotechnol* 16(1):1–20
- Cha YH, Kim NH, Park C, Lee J, Kim HS, Yook JI (2012) MiRNA-34 intrinsically links p53 tumor suppressor and Wnt signaling. *Cell Cycle* 11(7):1273–1281
- Gooneh-Farahani S, Naimi-Jamal MR, Naghib SM (2019) Stimuli-responsive graphene-incorporated multifunctional chitosan for drug delivery applications: a review. *Expert Opin Drug Deliv* 16(1):79–99
- Hemati M, Haghirsadat F, Jafary F, Moosavizadeh S, Moradi A (2019) Targeting cell cycle protein in gastric cancer with CDC20siRNA and anticancer drugs (doxorubicin and quercetin) co-loaded cationic PEGylated nanoniosomes. *Int J Nanomed* 14:6575–6585
- Krstic J, Galhuber M, Schulz TJ, Schupp M, Prokesch A (2018) p53 as a dichotomous regulator of liver disease: the dose makes the medicine. *Int J Mol Sci* 19(3):921
- Li XJ, Ren ZJ, Tang JH (2014) MicroRNA-34a: a potential therapeutic target in human cancer. *Cell Death Dis* 5(7):e1327–e1327
- Li G, Wang Z, Chong T, Yang J, Li H, Chen H (2017) Curcumin enhances the radiosensitivity of renal cancer cells by suppressing NF- κ B signaling pathway. *Biomed Pharmacother* 94:974–981
- Lin Y-L, Liu Y-K, Tsai N-M, Hsieh J-H, Chen C-H, Lin C-M, Liao K-W (2012) A Lipo-PEG-PEI complex for encapsulating curcumin that enhances its antitumor effects on curcumin-sensitive and curcumin-resistance cells. *Nanomedicine* 8(3):318–327
- Lv S, Tang Z, Li M, Lin J, Song W, Liu H, Huang Y, Zhang Y, Chen X (2014) Co-delivery of doxorubicin and paclitaxel by PEG-polypeptide nanovehicle for the treatment of non-small cell lung cancer. *Biomaterials* 35(23):6118–6129
- Majdzadeh M, Rezaei Zarchi S, Movahedpour AA, Shahi Malmir H, Sasani E, Haghirsadat BF (2018) A new strategy in improving therapeutic indexes of medicinal herbs: preparation and characterization of nano-liposomes containing *Mentha piperita* essential oil. *SSU J* 25(11):853–864

- Marta T, Luca S, Serena M, Luisa F, Fabio C (2016) What is the role of nanotechnology in diagnosis and treatment of metastatic breast cancer? Promising scenarios for the near future. *J Nanomater*. <https://doi.org/10.1155/2016/5436458>
- Mazidi Z, Javanmardi S, Naghib SM, Mohammadpour Z (2022) Smart stimuli-responsive implantable drug delivery systems for programmed and on-demand cancer treatment: an overview on the emerging materials. *Chem Eng J* 433:134569
- Moga MA, Bălan A, Dimienescu OG, Burtea V, Dragomir RM, Anastasiu CV (2019) Circulating miRNAs as biomarkers for endometriosis and endometriosis-related ovarian cancer—an overview. *J Clin Med* 8(5):735
- Naderinezhad S, Haghrosadat F, Amoabediny G, Naderinezhad A, Esmaili Z, Akbarzade A (2017) Synthesis of biodegradable and self-assembled anionic nano-carrier: novel approach for improvement of Curcumin- delivery to bone tumors cells & Mathematical modeling of drug-release kinetic. *NCMBJ* 7(27):77–84
- Naghib SM, Zare Y, Rhee KY (2020) A facile and simple approach to synthesis and characterization of methacrylated graphene oxide nanostructured polyaniline nanocomposites. *Nanotechnol Rev* 9(1):53–60
- Portnoy V, Huang V, Place RF, Li LC (2011) Small RNA and transcriptional upregulation. *Wires RNA* 2(5):748–760
- Rahimzadeh Z, Naghib SM, Askari E, Molaabasi F, Sadr A, Zare Y, Afsharpad M, Rhee KY (2021) A rapid nanobiosensing platform based on herceptin-conjugated graphene for ultrasensitive detection of circulating tumor cells in early breast cancer. *Nanotechnol Rev* 10(1):744–753
- Reid G, Kao SC, Pavlakis N, Brahmabhatt H, MacDiarmid J, Clarke S, Boyer M, van Zandwijk N (2016) Clinical development of TargomiRs, a miRNA mimic-based treatment for patients with recurrent thoracic cancer. *Epigenomics* 8(8):1079–1085
- Rygiel K (2017) Cardiotoxic effects of radiotherapy and strategies to reduce them in patients with breast cancer: an overview. *J Cancer Res Ther* 13(2):186
- Sadeghi M, Kashanian S, Naghib SM, Arkan E (2022a) A high-performance electrochemical aptasensor based on graphene-decorated rhodium nanoparticles to detect HER2-ECD oncomarker in liquid biopsy. *Sci Rep* 12(1):3299
- Sadeghi M, Kashanian S, Naghib SM, Askari E, Haghirsadat F, Tofighi D (2022b) A highly sensitive nanobiosensor based on aptamer-conjugated graphene-decorated rhodium nanoparticles for detection of HER2-positive circulating tumor cells. *Nanotechnol Rev* 11(1):793–810
- Sassen S, Miska EA, Caldas C (2008) MicroRNA—implications for cancer. *Virchows Arch* 452(1):1–10
- Urruticoechea A, Alemany R, Balart J, Villanueva A, Vinals F, Capella G (2010) Recent advances in cancer therapy: an overview. *Curr Pharm Des* 16(1):3–10
- Xiang Y, Guo Z, Zhu P, Chen J, Huang Y (2019) Traditional Chinese medicine as a cancer treatment: modern perspectives of ancient but advanced science. *Cancer Med* 8(5):1958–1975
- Yaghoubi F, Naghib SM, Motlagh NSH, Haghirsadat F, Jaliani HZ, Tofighi D, Moradi A (2021a) Multiresponsive carboxylated graphene oxide-grafted aptamer as a multifunctional nanocarrier for targeted delivery of chemotherapeutics and bioactive compounds in cancer therapy. *Nanotechnol Rev* 10(1):1838–1852
- Yaghoubi F, Motlagh NSH, Naghib SM, Haghirsadat F, Jaliani HZ, Moradi A (2022) A functionalized graphene oxide with improved cytocompatibility for stimuli-responsive co-delivery of curcumin and doxorubicin in cancer treatment. *Sci Rep* 12(1):1959

Publisher's Note

Springer Nature remains neutral with regard to jurisdictional claims in published maps and institutional affiliations.

Ready to submit your research? Choose BMC and benefit from:

- fast, convenient online submission
- thorough peer review by experienced researchers in your field
- rapid publication on acceptance
- support for research data, including large and complex data types
- gold Open Access which fosters wider collaboration and increased citations
- maximum visibility for your research: over 100M website views per year

At BMC, research is always in progress.

Learn more biomedcentral.com/submissions

